Hybrid Discontinuous/Boundary Conduction Mode of Flyback Microinverter for AC–PV Modules

Georgios C. Christidis, *Student Member, IEEE*, Anastasios Ch. Nanakos, and Emmanuel C. Tatakis

***Abstract*—The current-source flyback inverter has been proven an excellent solution for ac–PV modules. The two principal modes of operation of this converter are the discontinuous conduction mode (DCM) and the boundary conduction mode (BCM). Although BCM offers higher power density, it suffers at lower power levels, because of the significantly increased switching frequency that consequently leads to higher switching losses and lower overall converter efficiency. In this paper, a hybrid operating mode is presented, that combines both DCM and BCM during a utility grid period, so as to improve the converter performance as well as the efficiency and the power density on a wider power range. The mathematical analysis that describes the control specifics especially for a smooth transition between the two modes of operation is presented and demonstrated through computer simulations and experimental results on a laboratory prototype.**

***Index Terms*—AC–PV module, DC–AC power conversion, photovoltaic (PV) power systems, MIC, microinverter.**

NOMENCLATURE

α	Transition angle between DCM and i-BCM (rad).
δ_p	Peak duty cycle of DCM operation, referring to the switching cycle that would occur at $\omega t = \pi/2$.
$\delta_{\lim}$	Maximum duty cycle during DCM operation.
$f_{s,\mathrm{DCM}}$	Switching frequency of DCM operation (Hz).
$I_{\mathrm{pri},p,i}$	Peak current value of the transformer primary winding side during each switching cycle *i* (A).
$I_{\mathrm{pri,avg}}$	Average current value of the transformer primary winding side (A).
$I_{\mathrm{pri,avg,DCM}}$	Average current value of the transformer primary winding side when in DCM, during a utility grid half cycle (A).
$I_{\mathrm{pri,avg,crit}}$	Critical value of the average current of the transformer primary winding side in which hybrid mode begins (A).
k	Number of switching cycles during a utility grid half period when in DBCM operation.
λ	The ratio of V_{dc} to V_{acp}.
L_1	Transformer primary inductance (H).
l_g	Length of the core air gap (m).
m	Number of switching cycles during a utility grid half period when only in DCM operation.
n	Flyback transformer turns ratio.
N_{pri}	Number of turns of the transformer primary winding.
P_{PV}	Input power level of the converter, which is equal to the output power of the PV panel (W).
$P_{\mathrm{PV,nominal}}$	Nominal value of the PV panel power output (W).
$P_{\mathrm{PV,crit}}$	Critical value of the PV panel power output in which hybrid mode begins (W).
$t_{\mathrm{on},i}$	Primary switch on time during each switching cycle *i* (s).
$t_{\mathrm{off},i}$	Primary switch off time during each switching cycle *i* (s).
$t_{\mathrm{on},p}$	$t_{\mathrm{on},i}$ interval value referring to the switching cycle that occurs at the time-area of $\omega t = \pi/2$ for i-BCM (s).
T_{hl}	Rectified line period (s).
$T_{s,\mathrm{DCM}}$	Switching period of DCM operation (s).
V_{dc}	Input voltage of the inverter, which is equal to the PV output voltage (V).
V_{acp}	Peak voltage value of the utility grid (V).
$V_{\mathrm{ac},i}$	Mean voltage value of the utility grid during each switching cycle *i* (V).

Manuscript received April 20, 2015; revised July 3, 2015; accepted August 7, 2015. Date of publication August 19, 2015; date of current version January 7, 2016. Recommended for publication by Associate Editor T. Suntio.

G. C. Christidis and E. C. Tatakis are with the Laboratory of Electromechanical Energy Conversion, Department of Electrical and Computer Engineering, University of Patras, Rion-Patras 26504, Greece (e-mail: gchristidis@ece.upatras.gr; e.c.tatakis@ece.upatras.gr).

A. C. Nanakos was with the Laboratory of Electromechanical Energy Conversion, Department of Electrical and Computer Engineering, University of Patras, Rion-Patras 26504, Greece. He is now with Dyson Technology Ltd., Wiltshire, SN16 0RP, U.K. (e-mail: tnanakos@ece.upatras.gr).

Color versions of one or more of the figures in this paper are available online at http://ieeexplore.ieee.org.

Digital Object Identifier 10.1109/TPEL.2015.2470094

I. INTRODUCTION

POWER generation from renewable energy sources has gained an increased interest in the last few decades as a result of the price rise of fossil fuels, the increased power demand, as well as the growing environmental concerns [1], [2]. Solar energy has been in the center of attention, due to the recent advances in photovoltaic (PV) cells, which now offer increased energy conversion efficiency at a smaller purchase cost [3], [4]. Originally, the only cost-effective solution were large-scale, high-power PV plants, ranging up to several megawatts. However, the interest has gradually shifted to small-scale decentralized grid-connected PV systems, the latest technology of which is called the ac–PV module [5]–[11]. AC–PV modules integrate the power inverter to the back of each solar panel, creating as such an ac generator, which can be installed effortlessly and safely on any building's rooftop. Each module typically ranges from 50 to 400 W and the number of units installed depend on the available area and initial budget. The use of this technology guarantees maximum power generation under any weather condition or partial shadowing (since MPPT is applied to each solar panel individually), while at the same time being reliable and easily upgradable.

Among the many different converter topologies that have been proposed for use in ac–PV modules [12]–[15], the flyback current source inverter concentrates the research interest, since it satisfies the application requirements (high-voltage step-up ratio, electrical isolation, high power density, increased reliability, and low cost). The two most widely used operating modes of the flyback inverter are the discontinuous conduction mode (DCM) [16]–[18] and the boundary conduction mode (BCM) [16], [19]. An improved BCM modulation (i-BCM) was recently proposed in order to improve the output power quality of the flyback inverter [20], [21]. In both modes, the converter operates as a current source, rendering the control scheme fairly simple. In DCM, the switching frequency is constant and the flyback transformer is fully demagnetized before the next switching cycle, whereas in BCM, the transformer is momentarily demagnetized, leading to a variable switching frequency. Recently, the continuous conduction mode (CCM) was under evaluation by multiple research teams [22]–[25], which, due to the converter operation as a voltage source, demands a more complex control scheme for grid connection.

Comparing the two principal operating modes, DCM requires the least amount of hardware; however, its power density is limited [16]. On the other hand, although BCM is fairly more complicated, it can be implemented with [16], [21] or without [20] high-frequency sensors and can provide increased power density, since the transformer is continuously utilized. Nevertheless, its power efficiency is limited at lower PV irradiance levels, due to the increased switching frequency of the main transistor [16]. What is more, even in higher power levels, the switching losses during the time intervals close to the edges of the sinusoidal wave still remain unacceptable as will be shown in the next section.

In this paper, a hybrid operating mode of the flyback inverter combining DCM and i-BCM is proposed, which aims to increase the converter efficiency for a wide power range, without affecting the output power quality. Power quality has been a significant concern while investigating the use of multiple operating modes during a single utility grid cycle. For example, in [26]–[31] interleaved flyback topologies, in which one of the converters operate partially depending on the PV panel power output, are examined. The appropriate control method ensures smooth transition between the operating modes, limiting the total harmonic distortion (THD) of the output current and increasing the converter power factor.

The proposed hybrid operating mode in this paper combines both i-BCM (near the center of the sinusoidal wave) and DCM (during the rest of the period) during one utility grid half cycle and, depending on the PV power level, the utilization ratio of each mode varies. Thus, the proposed hybrid mode inherits the merits of both discrete modes, offering improved converter efficiency and higher power density. Comparing the proposed approach to the ones previously mentioned (see [22]–[25] and [26]–[31]), a flyback inverter operating in CCM requires high-frequency voltage and current sensors to implement the more complex control algorithm, than the one of a converter operating as a current source. What is more, the interleaved flyback topologies that were introduced may or may not require high-frequency sensors; however, they raise the complexity and cost of the converter and diminish their reliability.

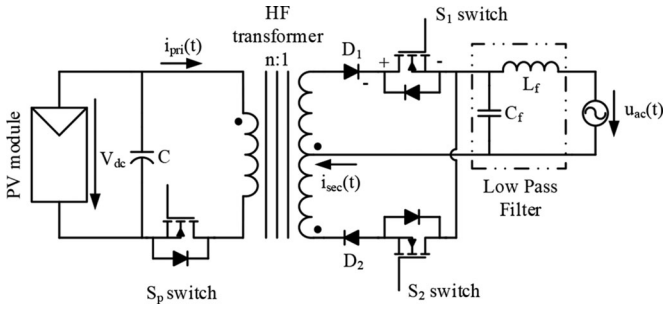

Fig. 1. Flyback inverter topology diagram.

In the following sections, the operating principle of the hybrid switching mode will be presented and compared to the existing DCM and i-BCM operating modes, followed by the analysis of the mathematical equations that describe the converter operation for any power level as well as the determination of the optimal transition point between the two operating modes. Results obtained by simulation analysis will show the converter operation for different power levels. Finally an experimental prototype is tested in order to validate the mathematical analysis, as well as to investigate the power efficiency increase by using the proposed hybrid operating mode.

II. Hybrid Switching Mode Operating Principle

The flyback inverter topology is shown in Fig. 1. S_P is the main semiconductor switch and operates in high frequency. The high-frequency transformer provides the electrical isolation and transfers the energy from the PV panel to the ac utility grid. Each transformer secondary winding operates during the appropriate utility grid half cycle, through the corresponding semiconductor switch S_1 or S_2. The flyback operation is ensured by the secondary winding diodes and the output current is injected to the grid through a low-pass filter.

In DCM, the switching frequency of S_P remains constant throughout a utility grid half cycle and the transistor on time is modulated sinusoidally [16], in order to achieve a sinusoidal output current waveform. In i-BCM, this is not the case, as the transformer must be demagnetized momentarily and so, both the switching frequency and the transistor on time are variable. By utilizing i-BCM the output current can remain sinusoidal at the expense of a more complicated control, as the envelope of the primary current for the two modes has different shape [20], [21]. Additionally, the switching frequency reaches its lowest value at the center of the sinewave, as shown in Fig. 2, which depicts the switching frequency of S_P during a line period for different PV power levels. As it is clearly shown from this figure, the switching frequency near the edges of the sinusoidal wave remains unacceptably high for a given power level. This leads not only to an even higher decrease of the power efficiency, but also to a problematic operation of the converter. Fig. 3 shows the minimum, maximum and average switching frequency as a function of the PV power level for a given flyback inverter operating in i-BCM. It is evident that, due to the increased switching

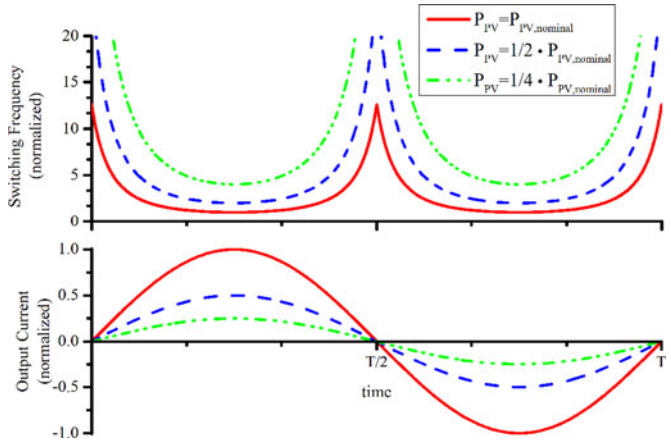

Fig. 2. Switching frequency and converter output current for different PV power levels for a flyback converter operated in i-BCM during a utility grid cycle.

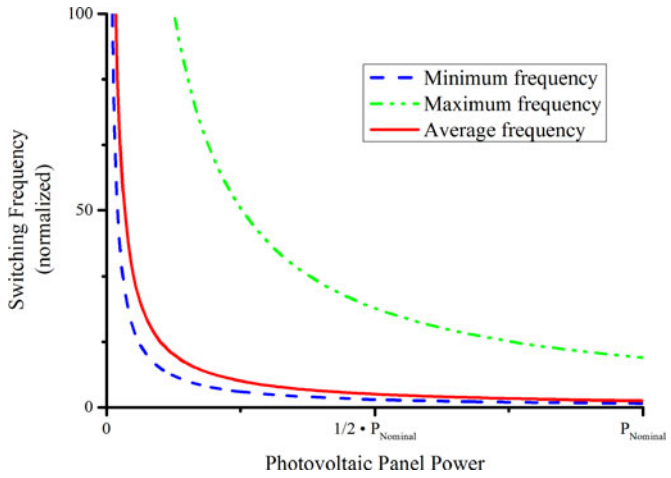

Fig. 3. Minimum, maximum, and average switching frequency as a function of the PV power level for a flyback converter operated in i-BCM.

frequency, at low PV irradiance levels, the converter suffers from high switching losses on S_P, diminishing the power efficiency of the PV system. Additionally, it is practically impossible to operate the converter at very low power levels given the frequency values needed for BCM. Moreover, even for higher PV power levels, the maximum switching frequency remains elevated, again decreasing the overall power efficiency. In DCM this problem is not present, due to the constant switching frequency. However, as the transformer is not fully utilized, the power density is limited compared to i-BCM, making a DCM inverter with the same specifications and performance larger, heavier and more expensive. In [16], the authors propose to operate the converter in DCM for lower PV levels (below 50% of the nominal power of the PV module) and in BCM for higher levels, to increase the overall efficiency. Nevertheless, even if this control mode overcomes one obstacle, the issue of the high switching frequency near the edges of the sinusoidal waveform at any power level still exists.

As a solution to the problems mentioned earlier, the hybrid DBCM switching mode is proposed in this paper. The converter

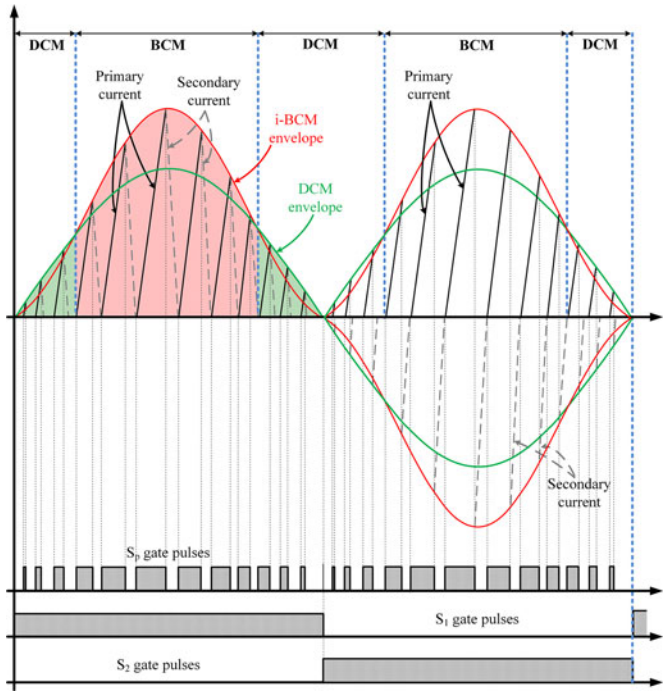

Fig. 4. Primary and secondary winding current waveforms and switching sequence diagram for hybrid DBCM.

operates in both DCM and i-BCM during the utility grid half cycle for high PV power levels, whereas it operates only in DCM under a critical PV power level $P_{\mathrm{PV,crit}}$. So, during a grid half cycle the DCM and i-BCM modes may coexist. The switching sequence of each semiconductor for this hybrid operating mode is presented in Fig. 4. As it is shown, the converter operates in i-BCM near the center of the sinusoidal wave, where the instantaneous output power is high, whereas near the edges it operates in DCM, with a constant switching frequency. As the power level decreases, the DCM operation percentage increases and if the PV power is lower than $P_{\mathrm{PV,crit}}$, then the converter operates fully in DCM. The switching frequency of the proposed hybrid mode is shown in Fig. 5 for different PV power levels.

The exact transition point along with the reference control signals for each operating mode are specified by the PV panel power level, together with the converter design parameters. It should be noted that an arbitrary selection of this point will not guarantee a smooth transition between the operating modes and will lead to an increased output current THD and lower power quality. Therefore, it is essential to accurately determine the control algorithm values based on the mathematical equations of the operating modes.

III. Mathematical Formulation

In this section, the analytical equations for the hybrid DBCM operation are described. For this analysis, it is considered that the grid voltage is sheer sinusoidal and that the switching frequency of S_P is a lot higher than the mains frequency. So, it can be assumed that the grid voltage during each switching cycle remains constant and equal to the value at the beginning of the

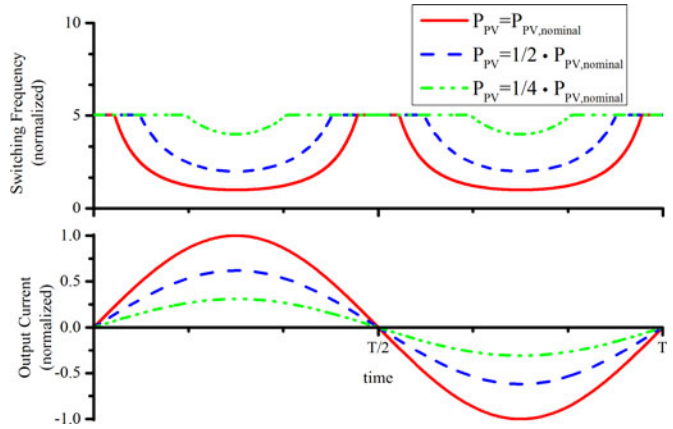

Fig. 5. Switching frequency and converter output current for different PV power levels for a flyback converter operated in hybrid DBCM during a utility grid cycle.

switching cycle

$$V_{\mathrm{ac},i} = V_{\mathrm{acp}}\sin(\omega t_{i-1}), \quad 0 \le i \le k. \tag{1}$$

If we assume that the transitions between DCM and i-BCM and vice versa, within the utility grid half period, occur at $\omega t_{i-1} = \alpha$ and $\omega t_{i-1} = \pi - \alpha$, respectively, then the converter operates in DCM for $0 < \omega t_{i-1} < \alpha$ and $\pi - \alpha < \omega t_{i-1} < p$, and in i-BCM for $\alpha < \omega t_{i-1} < \pi - \alpha$. Moreover, the values δ_p and $t_{\mathrm{on},p}$ determine the S_P pulsation for each mode of operation [16], [20]. So the problem is stated as follows:

Measuring the input power of the converter P_{PV}, the input and the peak output voltages V_{dc} and $V_{\mathrm{ac},p}$, for the given converter parameters, namely, n, $f_{s,\mathrm{DCM}}$, and L_1, calculate α, δ_p, and $t_{\mathrm{on},p}$ in order to achieve a sinusoidal output current as well as a smooth transition between the two modes of operation.

The first equation is established from the formula giving the input power of the converter

$$P_{\mathrm{PV}} = V_{\mathrm{dc}} \cdot I_{\mathrm{pri,avg}}. \tag{2}$$

So the average input current for the hybrid DBCM operation must be calculated. However, since the converter output current needs to be sinusoidal, and considering that there is no intermediate energy storage in the inverter, the form of the average input current per switching cycle is strictly determined (it follows a $\sin^2(\omega t)$ curve). What is more, this waveform must be independent of the mode of operation of the inverter (whether it is DCM, i-BCM, or even CCM). According to this consideration, the average input current per switching cycle for $\omega t_{i-1} = \pi/2$ must be the same with a matching converter that operates entirely in i-BCM, for the same power level. So, it is deduced that the input current peak level of the hybrid DBCM and i-BCM at $\omega t_{i-1} = \pi/2$ must be equal as well, which finally shows that the transistor on time at $\omega t_{i-1} = \pi/2$, $t_{\mathrm{on},p}$, can be calculated by the expression given for i-BCM [20]

$$I_{\mathrm{pri,avg}} = \frac{1}{4}\frac{V_{\mathrm{dc}}}{L_1}\frac{t_{\mathrm{on},p}}{1+(\lambda/n)} \Rightarrow P_{\mathrm{PV}} = \frac{1}{4}\frac{V_{\mathrm{dc}}^2}{L_1}\frac{t_{\mathrm{on},p}}{1+(\lambda/n)}. \tag{3}$$

Furthermore, in order to have a smooth transition, two conditions must be met at the transition points between DCM and i-BCM and vice versa, which, as already mentioned, will occur at $\omega t_{i-1} = \alpha$ and $\omega t_{i-1} = \pi - \alpha$.

First, the peak current of DCM and i-BCM operation must be equal during the transition, as shown in Fig. 4. It should be mentioned that the peak input current of the last switching cycle in DCM and the first switching cycle in i-BCM are considered to be equal based on the assumption that the switching period is a lot smaller than the utility grid half cycle period. So, since the peak input current is given by the equation

$$I_{\mathrm{pri},p,i} = \frac{V_{\mathrm{dc}}}{L_1} t_{\mathrm{on},i} \tag{4}$$

where

$$t_{\mathrm{on},i} = \delta_p \mathrm{T}_{s,\mathrm{DCM}} \sin(\omega t_{i-1}). \tag{5}$$

for DCM and

$$t_{\mathrm{on},i} = \frac{t_{\mathrm{on},p}}{1+(\lambda/n)} \sin\omega t_{i-1} \left(\sin(\omega t_{i-1}) + \frac{\lambda}{n}\right). \tag{6}$$

for i-BCM, using (5) and (6) for $\omega t_{i-1} = \alpha$, we conclude that

$$\begin{aligned} \frac{V_{\mathrm{dc}}}{L_1}\delta_p \mathrm{T}_{s,\mathrm{DCM}} \sin\alpha &= \frac{V_{\mathrm{dc}}}{L_1}\frac{t_{\mathrm{on},p}}{1+(\lambda/n)}\sin\alpha\left(\sin\alpha + \frac{\lambda}{n}\right) \\ \Rightarrow \delta_p \mathrm{T}_{s,\mathrm{DCM}} &= \frac{t_{\mathrm{on},p}}{1+(\lambda/n)}\left(\sin\alpha + \frac{\lambda}{n}\right). \end{aligned} \tag{7}$$

Second, during the transition, the sum of the switch-on time and switch-off time in DCM must be equal to the switching period of DCM. The off time in DCM is [16]

$$t_{\mathrm{off},i} = t_{\mathrm{off}} = \frac{\lambda}{n}\delta_p T_{s,\mathrm{DCM}}. \tag{8}$$

Accordingly for i-BCM, the off time is [20]

$$t_{\mathrm{off},i} = \frac{\lambda/n}{1+(\lambda/n)} t_{\mathrm{on},p}\left(\sin(\omega t_{i-1}) + \frac{\lambda}{n}\right). \tag{9}$$

Therefore

$$\begin{aligned} t_{\mathrm{on},i}|_{\omega t_{i-1}=\alpha} + t_{\mathrm{off},i}|_{\omega t_{i-1}=\alpha} &= T_{s,\mathrm{DCM}} \\ \delta_p T_{s,\mathrm{DCM}}\sin\alpha + \frac{\lambda}{n}\delta_p T_{s,\mathrm{DCM}} &= T_{s,\mathrm{DCM}} \\ \Rightarrow \delta_p\left(\sin\alpha + \frac{\lambda}{n}\right) &= 1. \end{aligned} \tag{10}$$

Equations (3), (7), and (10) describe a 3×3 system, from which it is possible to determine the parameters α, δ_p, and $t_{\mathrm{on},p}$ of a given converter, for any power level. The hybrid DBCM operation parameters are determined by solving the system of

TABLE I
INVERTER CHARACTERISTICS AND COMPONENT VALUES FOR THE PROPOSED HYBRID OPERATION

Nominal power: 200 W	$n = 0.314$	S_P : IXFH60N20	Core Type: ETD54 (3F3)
Input voltage: 25–40 V	$L_1 = 43\ \mu$H	S_1,S_2: IXFX26N120	$N_{\rm pri} = 22$
Output voltage: 230 V/50 Hz	$f_{S,\rm DCM} = 100$ kHz	Diode: RHR165120	$l_g = 0.395$ cm

equations mentioned earlier:

$$\begin{cases} \alpha = \arcsin\left(\dfrac{V_{\rm dc}}{2}\sqrt{\dfrac{\rm T_{s,DCM}}{P_{\rm PV}L_1}} - \dfrac{\lambda}{n}\right) \\ \delta_p = \dfrac{2}{V_{\rm dc}}\sqrt{\dfrac{P_{\rm PV}L_1}{\rm T_{s,DCM}}} \\ t_{{\rm on},p} = \dfrac{4P_{\rm PV}L_1}{V_{\rm dc}^2}\left(1+\dfrac{\lambda}{n}\right). \end{cases} \tag{11}$$

During the original DCM the maximum duty cycle occurs at $\omega t_{i-1} = \pi/2$. However, in the proposed hybrid DBCM operation, the maximum duty cycle $\delta_{\rm lim}$ occurs at the transition point between DCM and i-BCM, which can be calculated by using (10). More specifically

$$\begin{aligned} t_{{\rm on},i}|_{\omega t_{i-1}=\alpha} &= \delta_p T_{s,\rm DCM}\sin\alpha \\ \delta_{\rm lim}T_{s,\rm DCM} &= \frac{1}{\sin\alpha + (\lambda/n)}T_{s,\rm DCM}\sin\alpha \\ \delta_{\rm lim} &= \frac{\sin\alpha}{\sin\alpha + (\lambda/n)}. \end{aligned} \tag{12}$$

IV. DESIGN PROCEDURE AND APPLICATION ON A SPECIFIC MICROINVERTER

To validate the earlier equations, a 200-W flyback inverter is designed, which operates in the proposed hybrid DBCM, with input voltage operational levels from 25 to 40 V and output voltage 230 V/50 Hz.

In order to determine the design parameters and component values of the inverter, the constraints of the inverter operation must be taken into account, so as to ensure the feasibility of the design for the given specifications and establish that the components will operate within their safe operating area (SOA).

More specifically, for the transformer, the following limitations must be taken into consideration:

1) The peak flux density of the transformer core must be smaller than the manufacturer's maximum value to avoid saturation. For 3F3 cores, used in common flyback inverters, this value is 280 mT [32].
2) The area of primary and secondary windings divided by the transformer window (A_w) must be lower than the copper fill factor for the selected core. For economical transformer design (ETD) cores, this ratio is 0.35 [32].

Accordingly, for the power switches:

1) The peak voltage during operation must be lower than the breakdown voltage given by the manufacturer. The maximum breakdown voltage for power MOSFETs is selected to be 1200 V.

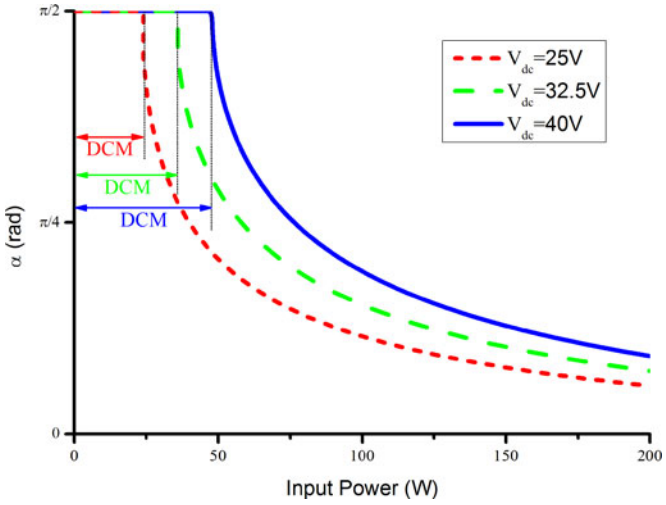

Fig. 6. Transition angle as a function of the input power level, for different input voltages.

2) The switching frequency of S_P has to be limited in order to avoid excessive switching losses on S_P and the diodes, as well as on the flyback transformer. Moreover, high switching frequency requires more complex and expensive components for the control circuit (microcontroller, isolation optocoupler, and MOSFET driver) and raises EMI. So, the maximum switching frequency of S_P is limited by the selection of the operating frequency when in DCM.

Based on the earlier converter specifications and constraints, the component values of the converter prototype used to validate the proposed hybrid operating mode were calculated based on [20] and are shown in Table I. The parameters α, δ_p, and $t_{{\rm on},p}$ are determined for the designed converter according to (11) and (12). Figs. 6–8 depict α, $\delta_{\rm lim}$, and $t_{{\rm on},p}$ as a function of the PV power level for three different input voltages.

For input power lower than the critical PV power level $P_{\rm PV,crit}$, the converter operates fully in DCM, as described in [16]. The critical PV power level is determined when $\alpha = \pi/2$. So, from (10), we have

$$\delta_p = \frac{1}{1+(\lambda/n)} \tag{13}$$

and consequently

$$\begin{aligned} P_{\rm PV,crit} &= V_{\rm dc}\cdot I_{\rm pri,avg,crit} = \frac{1}{4}\cdot V_{\rm dc}^2\cdot\frac{\delta_p^2\cdot T_{s,\rm DCM}}{L_1} = \\ &= \frac{1}{4}\cdot V_{\rm dc}^2\cdot\frac{T_{s,\rm DCM}}{L_1}\left[\frac{1}{1+(\lambda/n)}\right]^2. \end{aligned} \tag{14}$$

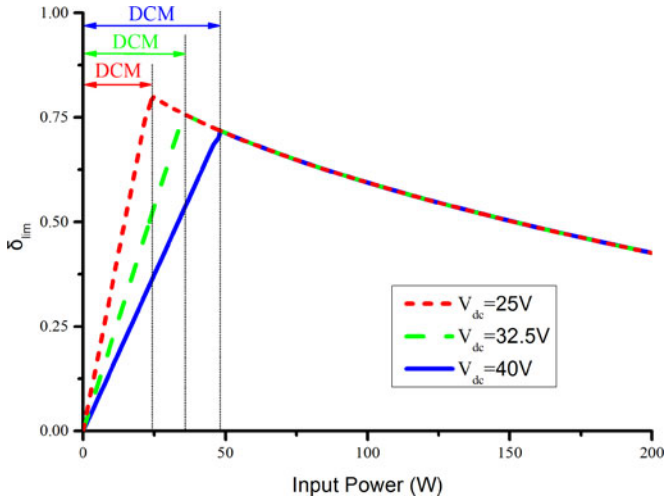

Fig. 7. Maximum duty cycle during DCM operation as a function of the input power level, for different input voltages.

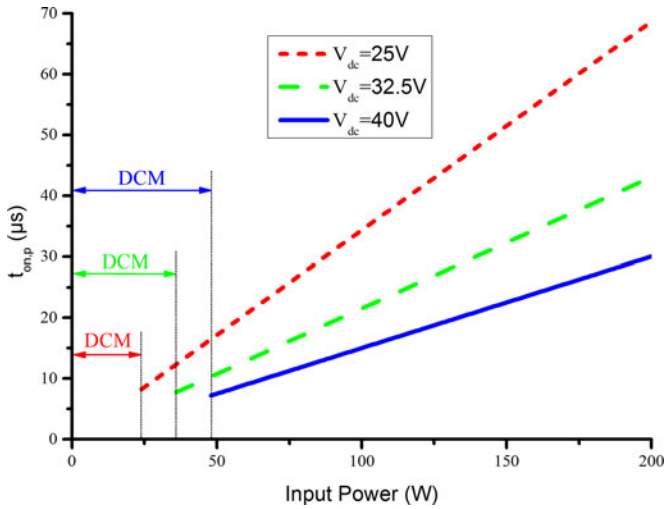

Fig. 8. Maximum on time during i-BCM operation as a function of the input power level, for different input voltages.

Therefore, for power levels lower than $P_{\mathrm{PV,crit}}$, the α remains $\pi/2$, indicating that there is no transition between the two modes of operation, δ_{lim} is proportional to the power level, and $t_{\mathrm{on},p}$ remains zero. The determination of $P_{\mathrm{PV,crit}}$, calculated in (14), is a function of the inverter design parameters and operating conditions (V_{dc}, L_1, λ, and n) and also the switching frequency when in DCM. As already explained, the aim of the proposed hybrid operating mode is to limit the maximum switching frequency of S_P, by forcing the converter to operate in DCM when the switching frequency reaches very high values. This frequency limit is selected empirically, based on the switching frequency value used in common flyback inverters for ac/PV modules, which varies between 20 and 100 kHz [16]–[18], [23], [25]–[27], [29]–[31], [33]–[38].

By examining the results, it is evident that as the power level increases, α decreases, meaning that the transition between DCM and i-BCM occurs sooner and that the converter operates for a greater percentage of time in i-BCM than in DCM. What is more, the critical power $P_{\mathrm{PV,crit}}$ before which the converter

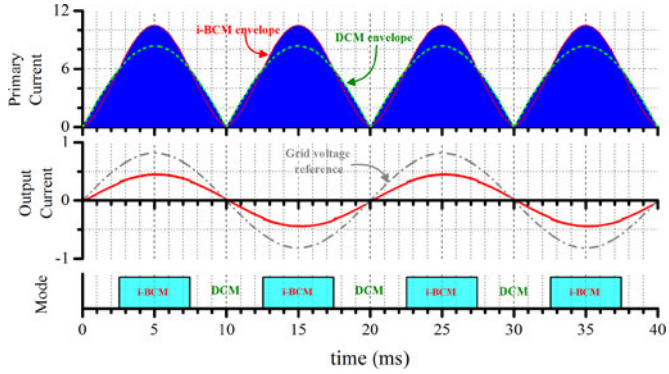

Fig. 9. Simulation results of the hybrid DBCM operation ($V_{\mathrm{dc}} = 40$ V, $P_{\mathrm{PV}} = 75$ W). Top to bottom: primary winding current, converter output current, and operating mode.

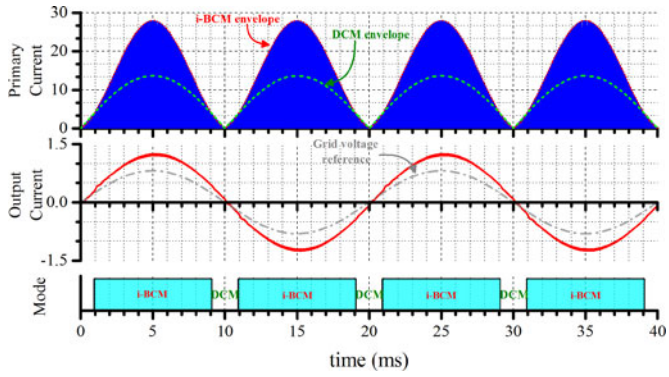

Fig. 10. Simulation results of the hybrid DBCM operation ($V_{\mathrm{dc}} = 40$ V, $P_{\mathrm{PV}} = 200$ W). Top to bottom: primary winding current, converter output current, and operating mode.

operates fully in DCM becomes lower as the input voltage drops. This is because the input current is higher, so the switching period of i-BCM that becomes equal to the DCM switching period occurs at a lower power level.

V. Simulation Results

Computer simulations of the proposed hybrid mode control were carried out in PSIM software to validate the earlier equations. Figs. 9 and 10 show the converter operation under two different input power levels for the same input voltage, whereas Fig. 11 depicts a magnification of the inverter operation during the transition between DCM and i-BCM. It is shown that as the power level increases, the transition between the two modes occurs sooner and the current envelope of i-BCM is significantly higher than the one of DCM. Furthermore, based on the output current waveform, it is evident that a smooth transition is accomplished, validating the derivation of the mathematical equations. Finally in Fig. 12, an application of the operation in DBCM where the two conditions for smooth transition are intentionally not met is depicted, in order to highlight the importance of a proper and thorough analysis needed for the appropriate behavior of the inverter. The transition occurs later than it should for the given power level, so there is a notable distortion in the converter output current, reducing its quality, even if the output power is the same. The THD of the output current is 7.26%,

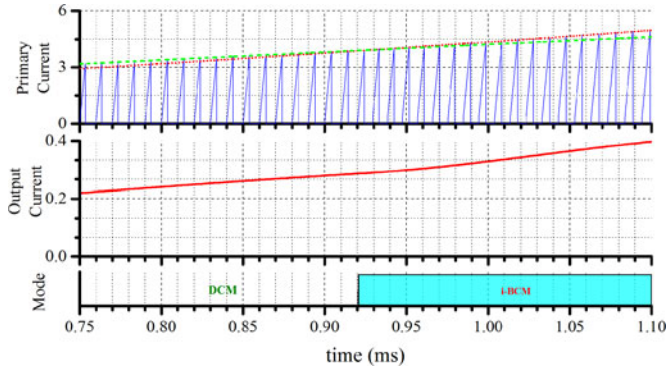

Fig. 11. Simulation results of the hybrid DBCM operation ($V_{\rm dc} = 40$ V, $P_{\rm PV} = 200$ W), magnified during the transition between DCM and i-BCM. Top to bottom: primary winding current, converter output current, and operating mode.

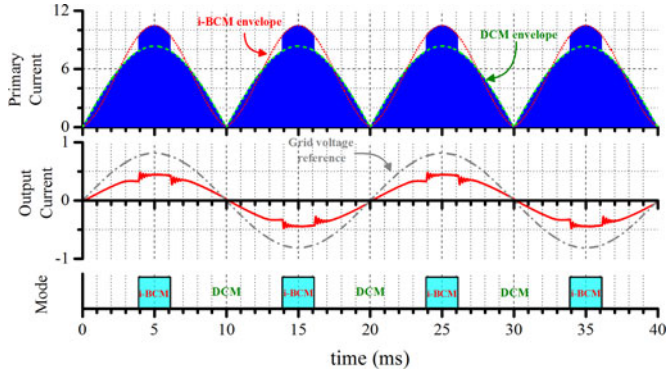

Fig. 12. Simulation results of an incorrect DBCM operation ($V_{\rm dc} = 40$ V, $P_{\rm PV} = 75$ W). Top to bottom: primary winding current, converter output current, and operating mode.

compared to 1.44% of the proposed operating mode for the same power level.

VI. Experimental Validation

A laboratory experimental prototype was built to validate the theoretical analysis of the hybrid modulation mode, as well as to determine the efficiency gain compared to DCM and i-BCM, using the components shown in Table I. The switching sequence, shown in Fig. 4, was implemented using a dsPIC30f4011 microcontroller, without the need of HF sensors, but instead, by predicting the on and off time of the switches. The simplified flowchart of the control algorithm implemented on the microcontroller is shown in Fig. 13. The microcontroller measures the input ($V_{\rm dc}$) and output ($V_{\rm ac}$) voltage. From the output voltage measurement, a zero cross algorithm determines the pulsation of the switches S_1 and S_2. From a peak detect algorithm, the microcontroller determines the hybrid operation parameters (α, δ_p, and $t_{{\rm on},p}$) for the given power level. Depending on the phase of the ac utility grid voltage, the microcontroller drives S_P based either on the DCM or on the i-BCM on and off time equations.

Figs. 14–17 depict the output current injected to the utility grid for different input power levels. It is evident that as the power level increases, the portion in which the converter operates in i-BCM becomes larger. However, for any power level, it is shown

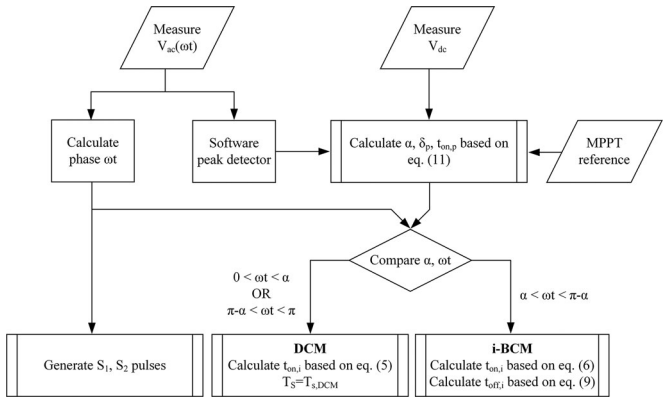

Fig. 13. Simplified flowchart of the microcontroller program implementing the proposed hybrid control.

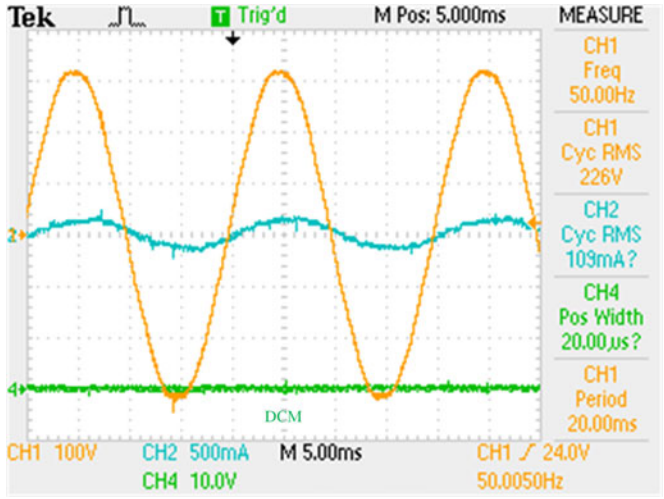

Fig. 14. Grid voltage and converter output current for $P_{\rm PV} = 25$ W and $V_{\rm dc} = 40$ V.

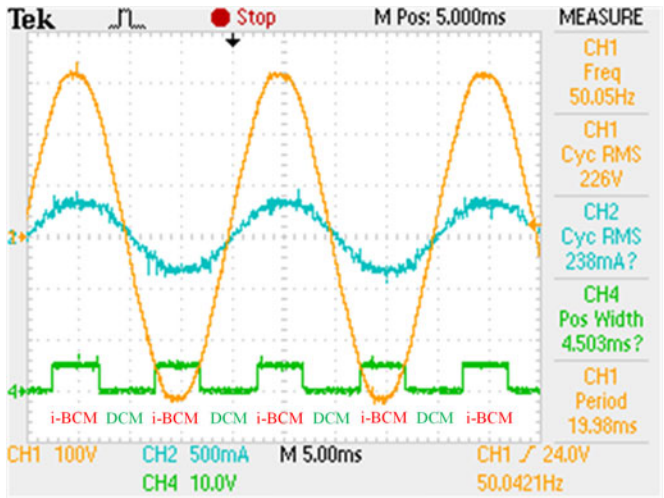

Fig. 15. Grid voltage and converter output current for $P_{\rm PV} = 60$ W and $V_{\rm dc} = 40$ V.

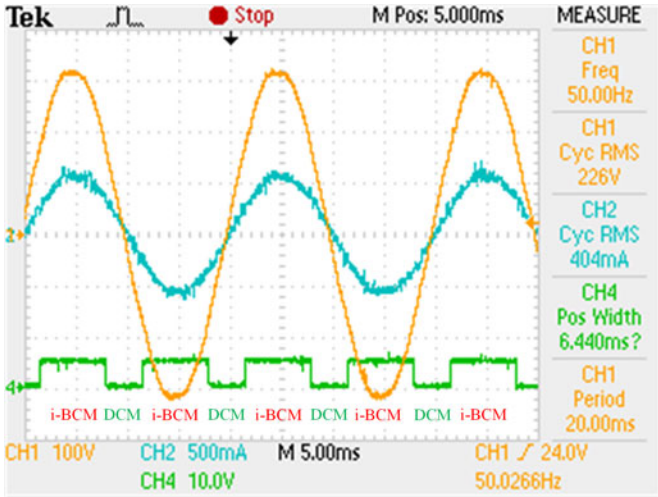

Fig. 16. Grid voltage and converter output current for $P_{\mathrm{PV}} = 100$ W and $V_{\mathrm{dc}} = 40$ V.

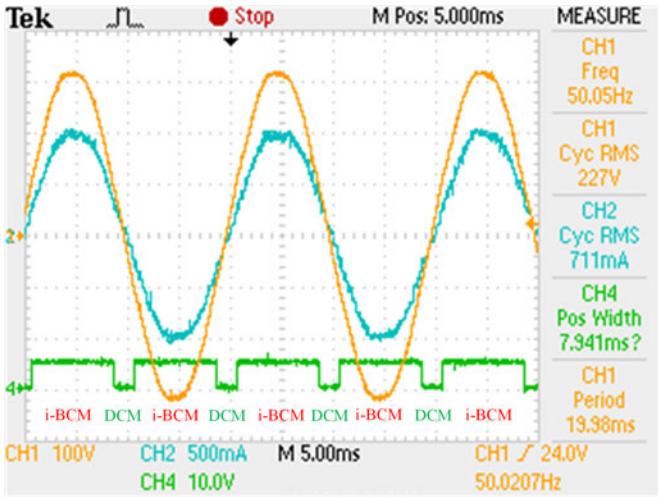

Fig. 17. Grid voltage and converter output current for $P_{\mathrm{PV}} = 180$ W and $V_{\mathrm{dc}} = 40$ V.

that the transition between the two modes is smooth. For very low power levels, the converter operates entirely in DCM, as shown in Fig. 14.

Having validated the feasibility of the proposed hybrid operating mode, it must now be compared to the existing operating modes of the flyback current source inverter, meaning DCM and i-BCM. Concerning the hardware complexity of the control circuit, the control algorithms for DCM and i-BCM are similar to the one used for the proposed hybrid mode, shown in Fig. 13.

While the converter designed using the components depicted in Table I can also operate in i-BCM, it cannot operate entirely in DCM for the whole power range. According to the equations found in [16] and [17], for the present converter, the switching frequency of DCM must be lower than 12.2 kHz. Switching frequencies higher than this will force the converter to operate in CCM in the center of the sinusoidal wave. This switching frequency is extremely low, making the output low-pass filter significantly larger, in order to operate within the limits of international standards that describe the connection of PV systems to utility grid [39], [40]. However, more importantly, for the same output filter, the breakdown voltage of S_1, S_2 must be greater than 1900 V (based on computer simulation results), due to the voltage fluctuation of the capacitor C_f of the output filter, making the operation of the current converter in DCM not feasible. Therefore, it is deduced that for comparison purposes, a new inverter for DCM operation must be designed from scratch. For this converter, the same ETD54 transformer core is selected. In order to guarantee the optimal selection of the design parameters, the algorithm described in [17] is used for the DCM converter. The components used for this converter are depicted in Table II.

To compare the power quality of the three operating modes, the THD of the output current is measured for different power levels and shown in Fig. 18. The DCM converter has the lowest THD value for any power level. This is due to the fact that it has the simplest control algorithm (the duty cycle is modulated sinusoidally and the switching frequency is constant) and the increased switching frequency makes best use of the low pass output filter. The converter operating in i-BCM has a larger THD value, which rises significantly as the input power decreases, because of the increased switching frequency near the edges of the sinusoidal wave. This switching frequency could reach several MHz, causing the decrease of the converter power quality (due to MOSFET switch-on and switch-off times, control circuit maximum operating frequency, and microcontroller quantization). On the other hand, the THD of the output current using the proposed control is slightly higher than the one when in DCM (0.2%–0.9%) due to the hybrid operation. During the measurements, the THD of the voltage the utility grid was 2.3%.

Finally, the comparison regarding the efficiency between the different modulation strategies is shown in Figs. 19–21 for different input voltages. In the same figures, the calculated percentage of the time period of DCM operation for the proposed hybrid mode is depicted, together with the calculated percentage of the power that it provides. Those values are given by

$$\text{DCM duration percentage} = \frac{2\alpha}{\pi} \tag{15}$$

$$\text{DCM power percentage} = \frac{V_{\mathrm{dc}} I_{\mathrm{pri,avg,DCM}}}{V_{\mathrm{dc}} I_{\mathrm{pri,avg}}} = \frac{I_{\mathrm{pri,avg,DCM}}}{I_{\mathrm{pri,avg}}}. \tag{16}$$

The calculation of $I_{\mathrm{pri,avg,DCM}}$ is found in the Appendix.

The precision power analyzer LMG500 of ZES Zimmer manufacturer was used to conduct precise power measurements.

As it can be observed, the efficiency using the proposed modulation is always higher than the one using i-BCM. This is especially true in the lower power levels where the improvement is more significant. This is due to the fact that in those lower power levels, the percentage of DCM operation is higher and so the maximum switching frequency is limited. This leads to a higher converter efficiency for a wider power range. What is more, the efficiency gain is more notable for higher input voltages, as the power percentage of DCM increases when the input voltage is increased. For higher power levels, as shown in Figs. 19–21, especially as the input voltage drops, the percentage of the converter operating in DCM is lower leading to

TABLE II
DCM INVERTER CHARACTERISTICS AND COMPONENT VALUES

Nominal Power: 200 W	$n = 0.370$	S_P : IXFH60N20	Core Type: ETD54 (3F3)
Input voltage: 25–40 V	$L_1 = 13.8\ \mu$H	S_1,S_2 : IXFX26N120	$N_{\rm pri} = 11$
Output voltage: 230 V/50 Hz	$f_{S,\rm DCM} = 36.98$ kHz	Diode: RHR165120	$l_g = 0.376$ cm

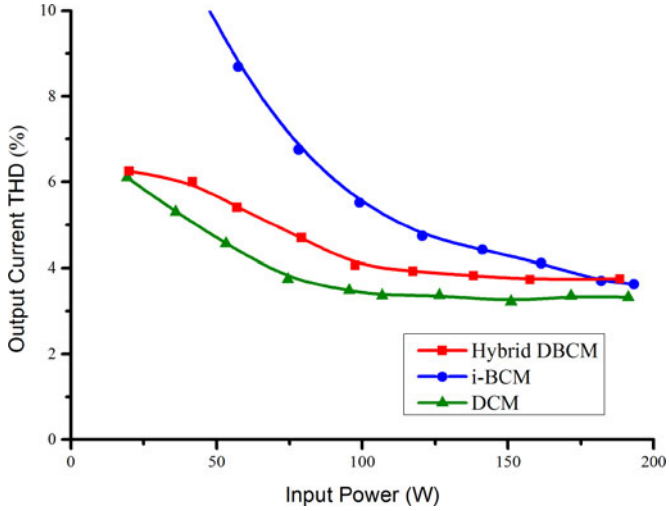

Fig. 18. THD of the converter output current of the proposed hybrid mode compared to i-BCM and DCM for $V_{\rm dc} = 40$ V.

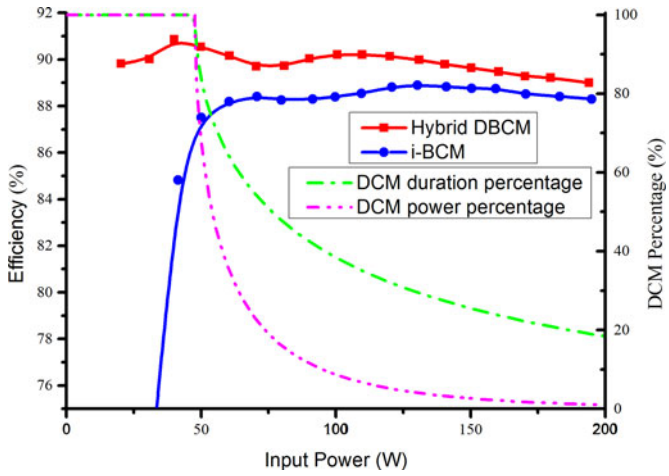

Fig. 19. Experimental efficiency measurement of the proposed hybrid mode compared to i-BCM and DCM for $V_{\rm dc} = 40$ V.

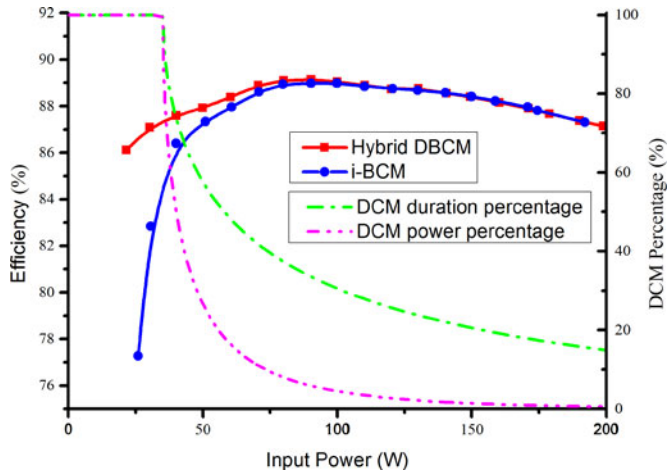

Fig. 20. Experimental efficiency measurement of the proposed hybrid mode compared to i-BCM and DCM for $V_{\rm dc} = 32.5$ V.

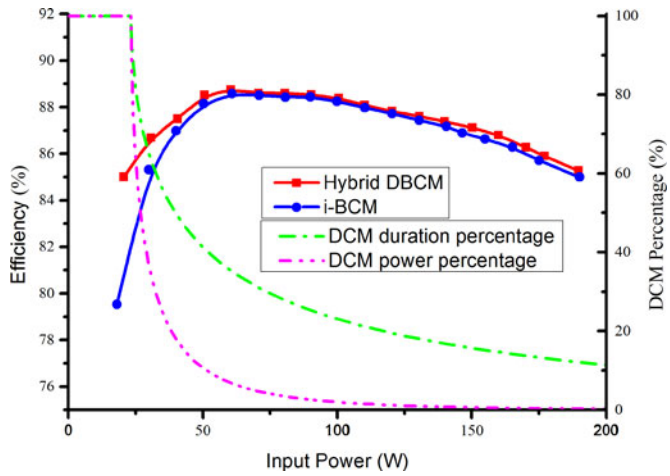

Fig. 21. Experimental efficiency measurement of the proposed hybrid mode compared to i-BCM and DCM for $V_{\rm dc} = 25$ V.

almost identical RMS values of the input and output currents. As a result, the efficiency gain is marginal. However, due to the nature of ac/PV modules and PV solar generation in general, the converter input power reaches its nominal value only for a limited time during a day, and therefore, it is of great importance that the designed converter achieves an improved efficiency for a wide input power range, corresponding to different irradiance levels.

Comparing the converter operating in the proposed hybrid mode with an equivalent converter operating in DCM, it is evident that the measured power efficiency is significantly higher for every power level and input voltage. This is justified by examining the converter design procedure for DCM. The wide input voltage and power range specifications, together with the design constraints analyzed in Section IV, lead to a DCM converter design with a smaller primary transformer inductance (a third of the one of the i-BCM/DBCM converter). This increases the RMS and peak values of the input and output currents for the same power level, increasing as a result the components conduction and switching losses. It should also be mentioned that the ratio of leakage inductance to primary inductance is much higher for the designed DCM transformer, contributing to the decrease of the power efficiency as well. The increased power losses cause not only a lower overall efficiency but also an increase of the converter cooling needs, decreasing as a result the power density. If a smaller transformer core was selected, to reduce the transformer mass and volume, the power

efficiency would be even lower. On the other hand, to match the efficiency performance with the one of the flyback inverter with the proposed hybrid operation, the DCM inverter could be designed with a larger transformer core, at the cost of a reduced power density.

VII. Conclusion

In this paper, a hybrid switching mode was proposed in which, depending on the input power level, the flyback inverter operates in DCM for one segment of the utility grid half cycle and in BCM for the rest. Since the converter operates always as a current source, the control is a lot simpler than using CCM. However, the switching period, which would reach high limits in the traditional BCM, is now limited, reducing the main transistor switching losses, which are quite significant at lower power levels. The analytical equations describing this operating mode were presented and calculated, highlighting the conditions that ensure a smooth transition between the two conduction modes. Simulation results demonstrated the importance of accurately calculating the control parameters to achieve good power quality. Finally, experimental results on a laboratory prototype validated the mathematical analysis and also showed an efficiency increase, especially in lower power levels, compared to the conventional DCM and BCM operations.

Appendix

The equations found in [16] are modified to calculate the average value of the input current for a section of the utility grid half cycle, corresponding to DCM operation. We can consider that the number of switching periods between 0 and α is $(\alpha/\pi)m$, and that, without significant error, this number is integer. So

$$I_{\mathrm{pri,avg,DCM}} = \frac{2}{T_{hl}} \int_0^{\alpha} i_{\mathrm{pri}}(t)dt = \frac{2}{T_{hl}} \sum_{i=1}^{(\alpha/\pi)m} \frac{V_{\mathrm{dc}}}{L_1} \frac{t_{\mathrm{on},i}^2}{2} \tag{17}$$

where in order to obtain a sinusoidal output current, $t_{\mathrm{on},i}$ should be given by

$$t_{\mathrm{on},i} = \delta_p T_{s,\mathrm{DCM}} \sin(\omega t_{i-1}) = \delta_p T_{s,\mathrm{DCM}} \sin\left(\frac{\pi}{m} i\right). \tag{18}$$

Combining (17) and (18), we obtain

$$\begin{aligned} I_{\mathrm{pri,avg,DCM}} &= \frac{2}{T_{hl}} \sum_{i=1}^{(\alpha/\pi)m} \frac{V_{\mathrm{dc}}}{2L_1} \delta_p^2 T_{s,\mathrm{DCM}}^2 \sin^2\left(\frac{\pi}{m} i\right) \\ &= \frac{2}{mT_{s,\mathrm{DCM}}} \frac{V_{\mathrm{dc}}}{2L_1} \delta_p^2 T_{s,\mathrm{DCM}}^2 \sum_{i=1}^{(\alpha/\pi)m} \sin^2\left(\frac{\pi}{m} i\right) \\ &= \frac{2V_{\mathrm{dc}}}{2mL_1 f_{s,\mathrm{DCM}}} \delta_p^2 \sum_{i=1}^{(\alpha/\pi)m} \sin^2\left(\frac{\pi}{m} i\right) \\ &= \frac{V_{\mathrm{dc}}\delta_p^2}{2L_1 f_{s,\mathrm{DCM}}} \left[\frac{2}{m} \sum_{i=1}^{(\alpha/\pi)m} \sin^2\left(\frac{\pi}{m} i\right)\right] \\ I_{\mathrm{pri,avg,DCM}} &= \frac{V_{\mathrm{dc}}\delta_p^2}{2L_1 f_{s,\mathrm{DCM}}} \Sigma_{2\alpha} \end{aligned} \tag{19}$$

where

$$\begin{aligned} \Sigma_{2\alpha} &= \frac{2}{m} \left[\sum_{i=1}^{(\alpha/\pi)m} \frac{1}{2} - \sum_{i=1}^{(\alpha/\pi)m} \frac{1}{2} \cos\left(\frac{2\pi}{m} i\right)\right] \\ &= \frac{2}{m}\frac{1}{2}\frac{\alpha}{\pi}m - \frac{2}{m}\frac{1}{2} \sum_{i=1}^{(\alpha/\pi)m} \cos\left(\frac{2\pi}{m} i\right) \\ &= \frac{\alpha}{\pi} - \frac{1}{m}\left[\frac{\sin\left[((\alpha/\pi)m + (1/2))\,(2\pi/m)\right]}{2\sin(\pi/m)}\right] \\ &= \frac{\alpha}{\pi} - \frac{1}{m}\left[\frac{\sin\left((\alpha/\pi)m(2\pi/m) + (1/2)(2\pi/m)\right)}{2\sin(\pi/m)}\right] \\ &= \frac{\alpha}{\pi} - \frac{1}{m}\frac{\sin(2\alpha + (\pi/m))}{2\sin(\pi/m)} \approx \frac{\alpha}{\pi} - \frac{1}{m}\frac{\sin(2\alpha)}{2(\pi/m)} \\ &= \frac{\alpha}{\pi} - \frac{\sin(2\alpha)}{2\pi}. \end{aligned} \tag{20}$$

So

$$I_{\mathrm{pri,avg,DCM}} = \frac{V_{\mathrm{dc}}\delta_p^2}{2L_1 f_{s,\mathrm{DCM}}} \left[\frac{\alpha}{\pi} - \frac{\sin(2\alpha)}{2\pi}\right]. \tag{21}$$

References

[1] B. K. Bose, "Global warming—Energy, environmental pollution and the impact of power electronics," *IEEE Ind. Electron. Mag.*, vol. 4, no. 1, pp. 6–17, Mar. 2010.

[2] F. Blaabjerg, Z. Chen, and S. B. Kjaer, "Power electronics as efficient interface in dispersed power generation systems," *IEEE Trans. Power Electron.*, vol. 19, no. 5, pp. 1184–1194, Sep. 2004.

[3] European Photovoltaic Industry Association (EPIA). (2014). *Global Market Outlook for Photovoltaics 2014–2018* [Online]. Available: http://www.epia.org/fileadmin/user_upload/Publications/44_epia_gmo_report_ver_17_mr.pdf

[4] European Photovoltaic Indusctry Association (EPIA). (2013). Global Market Outlook for Photovoltaics 2013-2017 [Online] http://www.epia.org/fileadmin/user_upload/Publications/GMO_2013_-_Final_PDF.pdf

[5] R. H. Wills, F. E. Hall, S. J. Strong, and J. H. Wohlgemuth, "The ac photovoltaic module," in *Proc. Conf. Rec. 25th IEEE Photovoltaic Spec. Conf.*, Washington, DC, USA, May 13–17, 1996, pp. 1231–1234.

[6] R. H. Wills, S. Krauthamer, A. Bulawka, and J. P. Posbic, "The AC photovoltaic module concept," in *Proc. 32nd IECEC*, 1997, vol. 3, pp. 1562–1563.

[7] J. Gow and C. Manning, "Photovoltaic converter system suitable for use in small scale stand-alone or grid-connected applications," *Proc. IEE -Electr. Power Appl.*, vol. 147, no. 6, pp. 535–543, Nov. 2000.

[8] Y. Xue, L. Chang, S. B. Kjaer, J. Bordonau, and T. Shimizu, "Topologies of single-phase inverters for small distributed power generators: An overview," *IEEE Trans. Power Electron.*, vol. 19, no. 5, pp. 1305–1314, Sep. 2004.

[9] J. J. Bzura, "The AC module: An overview and update on self-contained modular PV systems," in *Proc. 2010 IEEE Power Energy Soc. Gen. Meet.*, Jul. 25–29, 2010, pp. 1–3.

[10] B. Liu, S. Duan, and T. Cai, "Photovoltaic DC-building-module-based BIPV system—Concept and design considerations," *IEEE Trans. Power Electron.*, vol. 26, no. 5, pp. 1428–1429, May 2011.

[11] P. Mazumdar, P. N. Enjeti, and R. S. Balog, "Analysis and design of smart PV modules," *IEEE J. Emerg. Sel. Topics Power Electron.*, vol. 2, no. 3, pp. 451–459, Sep. 2014.

[12] S. B. Kjaer, J. K. Pedersen, and F. Blaabjerg, "A review of single-phase grid-connected inverters for photovoltaic modules," *IEEE Trans. Ind. Appl.*, vol. 41, no. 5, pp. 1292–1306, Sep./Oct. 2005.

[13] L. Quan and P. Wolfs, "A review of the single phase photovoltaic module integrated converter topologies with three dc link configurations," *IEEE Trans. Power Electron.*, vol. 23, no. 3, pp. 1320–1333, May 2008.

[14] D. Meneses, F. Blaabjerg, O. Garcia, and J. Cobos, "Review and comparison of step-up transformerless topologies for photovoltaic ac-module

application," *IEEE Trans. Power Electron.*, vol. 28, no. 6, pp. 2649–2662, Jun. 2013.
[15] T. Freddy, N. A. Rahim, W. P. Hew, and H. S. Che, "Comparison and analysis of single-phase transformerless grid-connected PV Inverters," *IEEE Trans. Power Electron.*, vol. 29, no. 10, pp. 5358–5369, Oct. 2014.
[16] A. Ch. Kyritsis, E. C. Tatakis, and N. P. Papanikolaou, "Optimum design of the current-source flyback inverter for decentralized grid-connected photovoltaic systems," *IEEE Trans. Energy Conv.*, vol. 23, no. 1, pp. 281–293, Mar. 2008.
[17] A. C. Nanakos, E. C. Tatakis, and N. P. Papanikolaou, "A weighted-efficiency-oriented design methodology of flyback inverter for ac photovoltaic modules," *IEEE Trans. Power Electron.*, vol. 27, no. 7, pp. 3221–3233, Jul. 2012.
[18] N. Kasa, T. Iida, and C. Liang, "Flyback inverter controlled by sensorless current mppt for photovoltaic power system," *IEEE Trans. Ind. Electron.*, vol. 52, no. 4, pp. 1145–1152, Aug. 2005.
[19] A. Ch. Kyritsis, N. P. Papanikolaou, E. C. Tatakis, and J. C. Kobougias, "Design and control of a current source flyback inverter for decentralized grid-connected photovoltaic systems," in *Proc. Eur. Conf. Power Electron. Appl.*, pp. 1–10, Sep. 2005, 11–14.
[20] A. C. Nanakos, G. C. Christidis, and E. C. Tatakis, "Weighted efficiency optimization of flyback micro-inverter under improved boundary conduction mode (i-BCM)," *IEEE Trans. Power Electron.*, vol. 30, no. 10, pp. 5548–5564, Oct. 2015.
[21] M. Gao, M. Chen, C. Zhang, and Z. Qian, "Analysis and implementation of an improved flyback inverter for photovoltaic ac module applications," *IEEE Trans. Power Electron.*, vol. 29, no. 7, pp. 3428–3444, Jul. 2014.
[22] F. F. Edwin, W. Xiao, and V. Khadikar, "Dynamic modeling and control of interleaved flyback module-integrated converter for PV power applications," *IEEE Trans. Ind. Electron.*, vol. 61, no. 3, pp. 1377–1388, Mar. 2014.
[23] Y.-H. Ji, D.-Y. Jung, J.-H. Kim, T.-W. Lee, and C.-Y. Won, "A current shaping method for PV-AC module DCM-flyback inverter under CCM operation," in *Proc. IEEE 8th Int. Conf. Power Electron. ECCE Asia*, pp. 2598–2605, 2011, 30 May–3 Jun.
[24] Y. Li and R. Oruganti, "A low cost flyback CCM inverter for AC module application," *IEEE Trans. Power Electron.*, vol. 27, no. 3, pp. 1295–1303, Mar. 2012.
[25] T. V. Thang, N. M. Thao, J.-H. Jang, and J.-H. Park, "Analysis and design of grid-connected photovoltaic systems with multiple-integrated converters and a pseudo-DC-link inverter," *IEEE Trans. Ind. Electron.*, vol. 61, no. 7, pp. 3377–3386, Jul. 2014.
[26] Y.-C. Hsieh, M.-R. Chen, and H.-L. Cheng, "An interleaved flyback converter featured with zero-voltage transition," *IEEE Trans. Power Electron.*, vol. 26, no. 1, pp. 79–84, Jan. 2011.
[27] Y.-H. Kim, Y.-H. Ji, J.-G. Kim, Y.-C. Jung, and C.-Y. Won, "A new control strategy for improving weighted efficiency in photovoltaic AC module-type interleaved flyback inverters," *IEEE Trans. Power Electron.*, vol. 28, no. 6, pp. 2688–2699, Jun. 2013.
[28] Z. Zhang, M. Chen, W. Chen, and Z. Qian, "Design and analysis of the synchronization control method for BCM/DCM current-mode flyback micro-inverter," in *Proc. 2013 28th Annu. IEEE Appl. Power Electron. Conf. Expo.*, pp. 68–75, Mar. 17–21, 2013.
[29] Z. Zhang, X.-F. He, and Y.-F. Liu, "An optimal control method for photovoltaic grid-tied-interleaved flyback microinverters to achieve high efficiency in wide load range," *IEEE Trans. Power Electron.*, vol. 28, no. 11, pp. 5074–5087, Nov. 2013.
[30] B. Tamyurek and B. Kirimer, "An interleaved high-power flyback inverter for photovoltaic applications," *IEEE Trans. Power Electr.*, vol. 30, no. 6, pp. 3228–3241, Jun. 2015.
[31] Y.-H. Kim, J.-W. Jang, S.-C. Shin, and C.-Y. Won, "Weighted-efficiency enhancement control for a photovoltaic AC module interleaved flyback inverter using a synchronous rectifier," *IEEE Trans. Power Electr.*, vol. 29, no. 12, pp. 6481–6493, Dec. 2014.
[32] L. H. Dixon, *Magnetics Design for Switching Power Supplies.* Dallas, TX, USA: Unitrode Seminars (TI), 2001.
[33] D. K. Ryu, Y. H. Kim, J. G. Kim, C. Y. Won, and Y. C. Jung, "Interleaved active clamp flyback inverter using a synchronous rectifier for a photovoltaic AC module system," in *Proc. IEEE 8th Int. Conf. Power Electron. ECCE Asia*, pp. 2631–2636, May 30–Jun. 3, 2011.
[34] H. Hu, S. Harb, X. Fang, D. Zhang, Q. Zhang, Z. J. Shen, and I. Batarseh, "A three-port flyback for PV microinverter applications with power pulsation decoupling capability," *IEEE Trans. Power Electr.*, vol. 27, no. 9, pp. 3953–3964, Sep. 2012.
[35] Y.-S. Noh, M.-N. Kim, J.-G. Kim, C.-Y. Won, and Y.-C. Jung, "Analysis and design of decoupling capacitor for single phase flyback-inverter with active power decoupling circuit," in *Proc. IEEE Int. Symp. Ind. Electron.*, pp. 1–6, May 28–31, 2013.
[36] Y.-H. Kim, J.-W. Jang, Y.-C. Jung, D.-K. Ryu, and C.-Y. Won, "High efficiency design method for photovoltaic AC module system of 250W," in *Proc. IEEE Int. Symp. Ind. Electron.*, pp. 1–6, May 28–31, 2013.
[37] S. Zengin and M. Boztepe, "Variable switching frequency operation of DCM flyback micro-inverter," in *Proc. 8th Int. Conf. Elect. Electron. Eng.*, pp. 102–106, Nov. 28–30, 2013.
[38] N. Sukesh, M. Pahlevaninezhad, and P. K. Jain, "Analysis and implementation of a single-stage flyback PV microinverter with soft switching," *IEEE Trans. Ind. Electron.*, vol. 61, no. 4, pp. 1819–1833, Apr. 2014.
[39] *Characteristics Utility Interface Photovoltaic (PV) Systems*, IEC 61727, 2004.
[40] *IEEE Standard Interconnecting Distributed Resources With Electric Power Systems,* IEEE Std. 1547, 2003.

Georgios C. Christidis (S'10) received the Diploma degree in electrical and computer engineering from the University of Patras, Rion-Patras, Greece, in 2010, where he is currently working toward the Ph.D. degree in voltage step-up converters.

His current research interests include the analysis, design, simulation, and construction of dc/dc and dc/ac converters for use in renewable energy systems, waste heat recovery systems, and aeronautics and space applications.

Mr. Christidis is a Member of the Technical Chamber of Greece.

Anastasios Ch. Nanakos was born in Thessaloniki, Greece, in 1981. He received the Dipl. and the Ph.D. degrees from the University of Patras, Patras, Greece, in 2005 and 2012, respectively, both in electrical and computer engineering.

He was a Researcher and Teaching Assistant at the University of Patras and as a Laboratory Collaborator at the Technological Educational Institute of Patras. He is currently with Dyson Technology Ltd., Wiltshire, U.K. His current research interests include power electronic converters, electric motor drives, design optimization techniques, and other related topics.

Emmanuel C. Tatakis received the Diploma in electrical engineering from the University of Patras, Rion-Patras, Greece, in 1981, and the Ph.D. degree in applied sciences from the University of Brussels, Brussels, Belgium, in 1989.

He is currently a Professor with the Department of Electrical and Computer Engineering, University of Patras. His teaching activities include power electronics and electrical machines. His current research interests include switch-mode power supplies, resonant converters, HF transformers, power factor correction, electric drive systems and electric vehicles, converters for renewable energy systems, voltage multipliers, educational methods in electrical machines, and power electronics.

Dr. Tatakis is a Member of the European Power Electronics Association (EPE) and the Technical Chamber of Greece.